Electronic Supplementary Material (ESI) for ChemComm.

Supporting information

Unique lithium precipitation behavior inside Li_3PS_4 solid electrolyte observed via multimodal/multiscale *operando* X-ray computed tomography

Jaehee Park[1], Toshiki Watanabe[1*], Seunghoon Yang[1], Kentaro Yamamoto[1,2], Tomoki Uchiyama[1], Tsuyoshi Takami[1], Atsushi Sakuda[3], Akitoshi Hayashi[3], Masahiro Tatsumisago[3], Yoshiharu Uchimoto[1]

[1] Graduate School of Human and Environmental Studies, Kyoto University, Kyoto 606-8501, Japan

[2] Faculty of Engineering, Nara Women's University, Kita Uoya Higashimachi, Nara 630-8506, Japan

[3] Department of Applied Chemistry, Graduate of School Engineering, Osaka Metropolitan University, Sakai, Osaka 599-8531, Japan

EXPERIMENTAL METHODS

1. Material preparation

Li_3PS_4 glass was prepared using a mechanical milling method. Stoichiometric amounts of Li_2S (Sigma-Aldrich, >99.9%) and P_2S_5 (Sigma-Aldrich, 99%) were mixed using an agate mortar and pestle, and the mixture was mechanically milled at 600 rpm for 20 h using a ZrO_2 pot with ZrO_2 balls (60 g). Powder X-ray diffraction (XRD, CuKα, 45 kV, 40 mA) patterns were recorded using an RINT-Ultima III (Rigaku) to verify the amorphous structure of Li_3PS_4 at room temperature. An Ar-filled sample holder was used to prevent degradation due to moisture. Raman spectra of the Li_3PS_4 powders were obtained using a DXR3 Smart Raman spectrometer (Thermo Fisher Scientific) with a 532 nm diode-pumped solid-state laser. Furthermore, scanning electron microscopy (SEM) was conducted using a Hitachi SU8220 to observe Li_3PS_4.

2. Galvanostatic cycling tests

Li/Li_3PS_4/Li cells with a diameter of 10 mm were constructed for electrochemical measurements in an argon-filled glove box. Li_3PS_4 pellets were prepared by pressing Li_3PS_4 powder uniaxially at 360 MPa. Li foils was attached to both sides of the Li_3PS_4 pellets and Cu current collectors were placed on the Li foils. Galvanostatic cycling tests were conducted for the symmetric cells at various current densities at 25°C.

3. Ionic and electronic conductivity measurements

Dense Li_3PS_4 pellets with a thickness of 0.8 mm and diameter of 10 mm were prepared for ionic conductivity measurements by pressing the Li_3PS_4 powder using stainless steel bars from both sides at 360 MPa in an argon-filled glove box. The ionic conductivity of Li_3PS_4 was measured using electrochemical impedance spectroscopy with an amplitude of 10 mV and frequency of 1 MHz to 0.1 Hz at 25°C. Equal amount of Li_3PS_4 pellets were prepared for electronic conductivity measurements by pressing Li_3PS_4 powder sandwiched with Cu foil from both sides using stainless steel bars at 360 MPa in an argon-filled glove box. The electronic conductivity of Li_3PS_4 at 25°C was measured by applying a direct current voltage of 0.1 V to the Cu/Li_3PS_4/Cu cell.

4. X-ray absorption spectroscopy (XAS)

The XAS spectra of the Li/Li_3PS_4/Li cells before and after short-circuiting by critical current density (CCD) testing were measured using the partial fluorescence yield method at beamline BL27SU at SPring-8 (Japan).

5. *Operando* X-ray computed tomography (CT) measurements

A homemade electrochemical cell with an inner diameter of 1 mm, shown in Figure S3, was used for the *operando* CT measurements. In a glove box with an Ar atmosphere controlled below the dew point of -90°C, Li_3PS_4 was filled into the homemade cell and sandwiched between Li metal to construct a Li/Li_3PS_4/Li symmetric cell. Then, the homemade cell was tightly sealed with an O-ring to avoid contact of the Li and Li_3PS_4 with air (see FigureS8). After taking the homemade cell from the glove box, the *operando* CT measurements were conducted with an X-ray energy of 15 keV without air exposure at beamline BL20XU at SPring-8, Japan. The CT images were collected immediately every 30 min during plating at 0.8 mA cm^{-2} with micro- and nanoscale modes, which have different spatial resolutions. The CT image with the micro-scale mode was obtained using absorption-contrast mode with a charge-coupled device camera (2048 × 2048 pixels); 1800 radiographs were collected using an exposure time of 30 ms during 180° rotation. The field of view at the micro-scale was 1 mm × 1 mm and the resolution was 1 μm. The CT image with the nano-scale mode was obtained using a microscope system with a condenser and zone plate. The images were collected using absorption-contrast and phase-contrast methods with a charge-coupled device camera; 1800 radiographs were collected using an exposure time of 500 ms with 180° rotation. The field of view at the nano-scale was 65 μm × 65 μm and the voxel size was 64 nm. After a series of data processing steps, the shadow images were converted into cross-sectional slices, which were then stacked together to render a three-dimensional (3D) reconstruction of the cell.

Reductive decomposition of Li_3PS_4

When Li_3PS_4 is reductively decomposed into Li_3P and Li_2S, the reaction equation considered is Equation S1 shown below. The respective densities are 1.85 for Li_3PS_4, 1.67 for Li_2S, and 1.48 g/cm^3 for Li_3P.[1] Calculating from these values, the volume of Li_3PS_4 expands about 1.5 times after decomposition. The porosity of the electrolyte layer from the CT image to 0-1.5 h, when Li deposition begins, is shown in Figure S5. The formation of decomposition products causes the volume to expand and the porosity to decrease.

$$Li_3PS_4 + 8\ Li^+ + 8\ e^- \rightarrow 4\ Li_2S + Li_3P \qquad \text{(Equation S1)}$$

Influence of secondary particle systems on Li_3PS_4

To examine the effect of the secondary particle size and compaction density of Li_3PS_4 and CCD of the solid electrolyte layer, a liquid phase method was used to synthesize Li_3PS_4 with a smaller secondary particle size than that obtained by mechanical milling Li_3PS_4.[2] Figure S9 shows SEM images of the solid-phase synthesized Li_3PS_4 and the liquid phase synthesized Li_3PS_4 as well as CT images of the electrolyte layers of these electrolytes compressed at 360 MPa. The secondary particle size of the Li_3PS_4 by using liquid phase synthesis was approximately 1–2 μm from SEM image, which was smaller than that (10–50 μm) of the Li_3PS_4 by using mechanical milling method (Figure S9a and b). The CT images showed that the average void ratio in the solid electrolyte layer of the solid-phase synthesized Li_3PS_4 was 0.47%, which value was larger than that of the liquid-phase synthesized Li_3PS_4 (0.42%). The CCD tests were performed with Li/solid electrolyte/Li cells using these two kinds of electrolytes, which have different average void ratio in the solid electrolyte layer (Figure S10 In the CCD tests charge/discharge cycles were performed while increasing the current density until a short circuit occurred, and the current density just before the short circuit occurred was defined as CCD. The CCD value of the symmetric cell using the Li_3PS_4 with relatively high void ratio (0.47%) was 0.32 mA cm^{-2}, and which was same as that of the symmetric cell using the Li_3PS_4 with relatively low void ratio (0.42%). These results suggest that the density of the electrolyte layer increases with decreasing the particle size of the solid

electrolyte, but the density difference does not affect the lithium dendrite formation speed. This is probably because the Young's modulus of Li_3PS_4 is small of 23 GPa[3], and thus the dense solid electrolyte

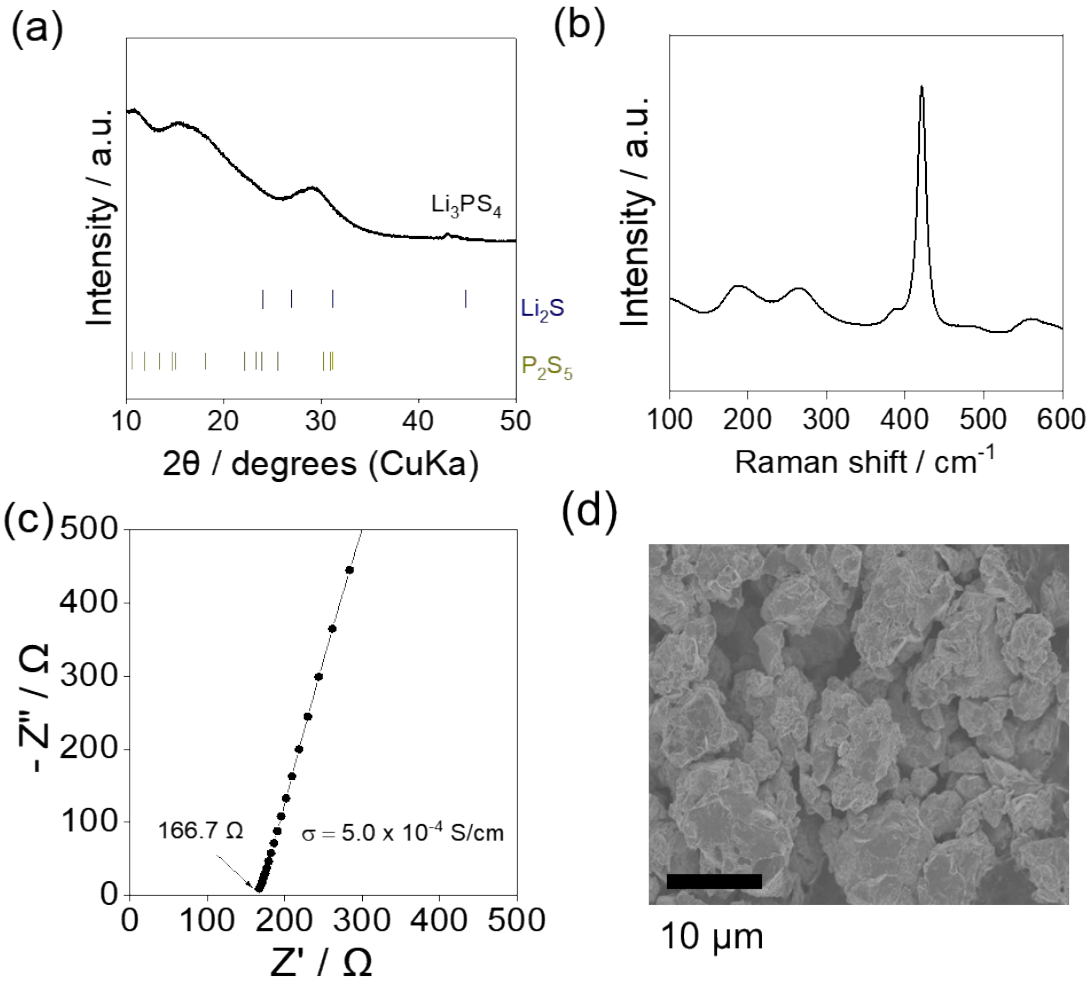

Figure S1. (a) The XRD pattern for amorphous Li_3PS_4. (b) Raman spectrum between 300 and 500 cm^{-1} of the Li_3PS_4 powder sample. (c) The Nyquist plot of Li_3PS_4 solid electrolyte. (d) SEM image showing morphology of Li_3PS_4.

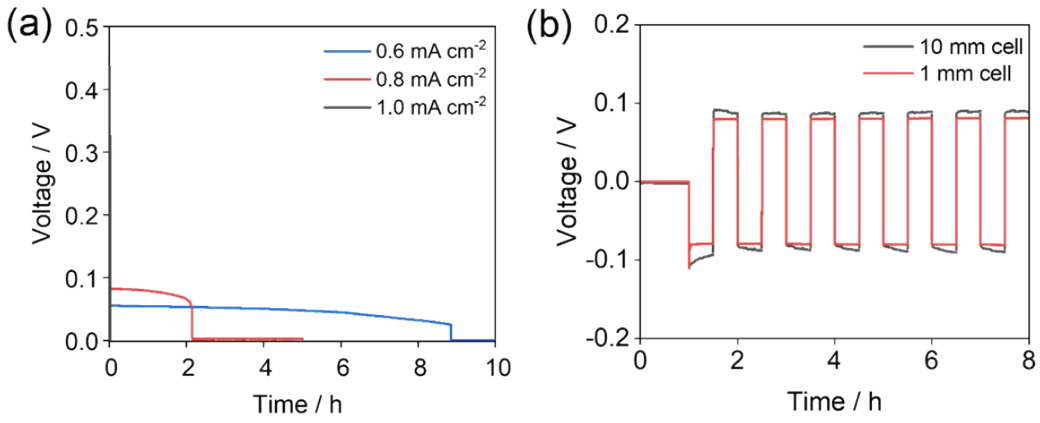

Figure S2. (a) Galvanostatic lithium plating of a Li/Li_3PS_4/Li symmetric cell (diameter of 1 mm) at 25°C at current densities of 1.0, 0.8, and 0.6 $mAcm^{-2}$. (b) Results of galvanostatic lithium deposition-stripping test for Li/Li_3PS_4/Li symmetric cells (diameter of 10 or 1 mm) at a constant current density of 0.8 mA cm^{-2} at 25°C, showing that the two cells were nearly identical.

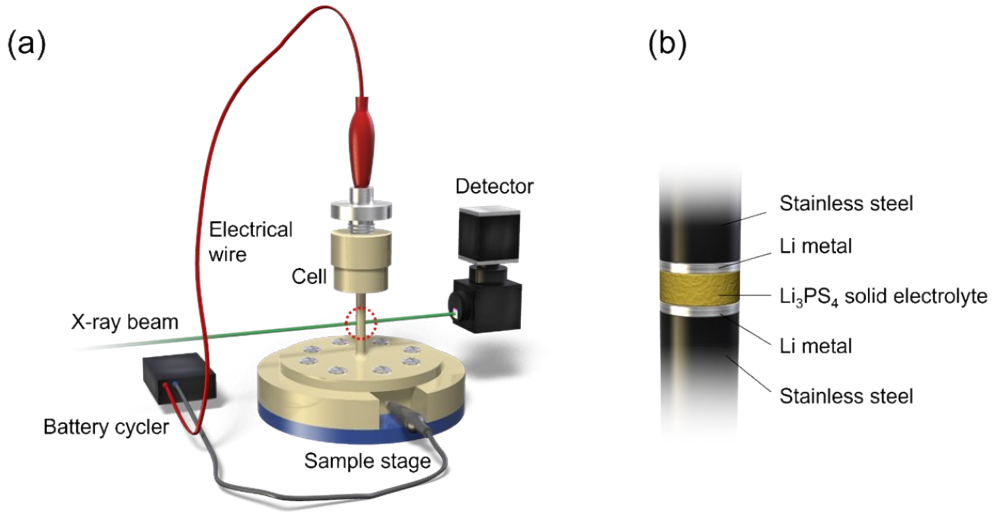

Figure S3. (a) Schematic depiction of the experimental beamline setup for operando X-ray CT. (b) Magnified image of the in-operando cell (diameter of 1 mm) for synchrotron X-ray CT.

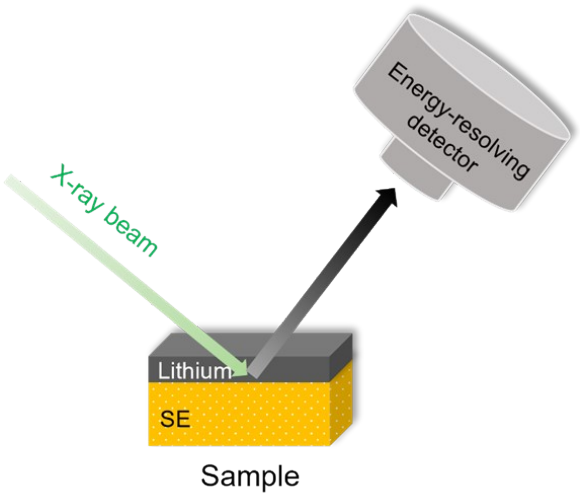

Figure S4. Schematic diagram of the PFY-XAS measurement setup using a synchrotron X-ray beam.

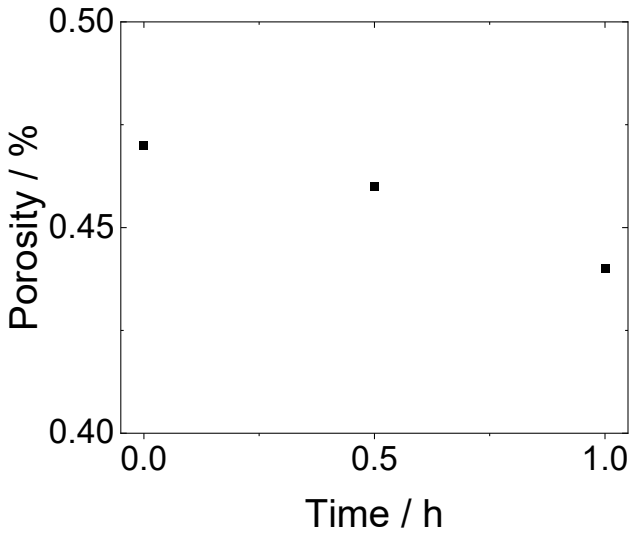

Figure S5. Quantitative analysis of the porosity in Li_3PS_4 measured from tomography. Each point represents porosity of the solid electrolyte at different times during the experiment in Figure 2a, and shows the void percentage of the total volume of the solid electrolyte at a given time.

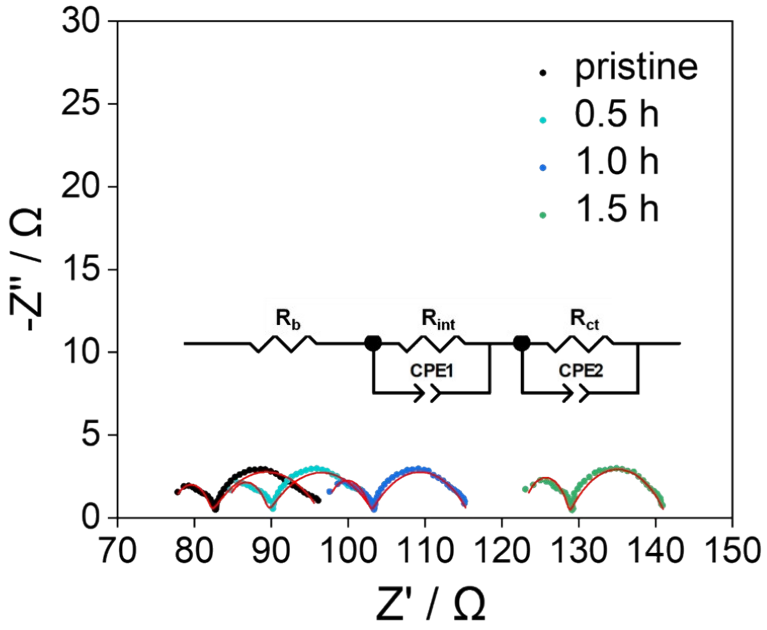

Figure S6. Nyquist plots and equivalent circuit fits of the pristine cell, after 0.5 h, after 1.0 h, and after 1.5 h based on data from Table S2.

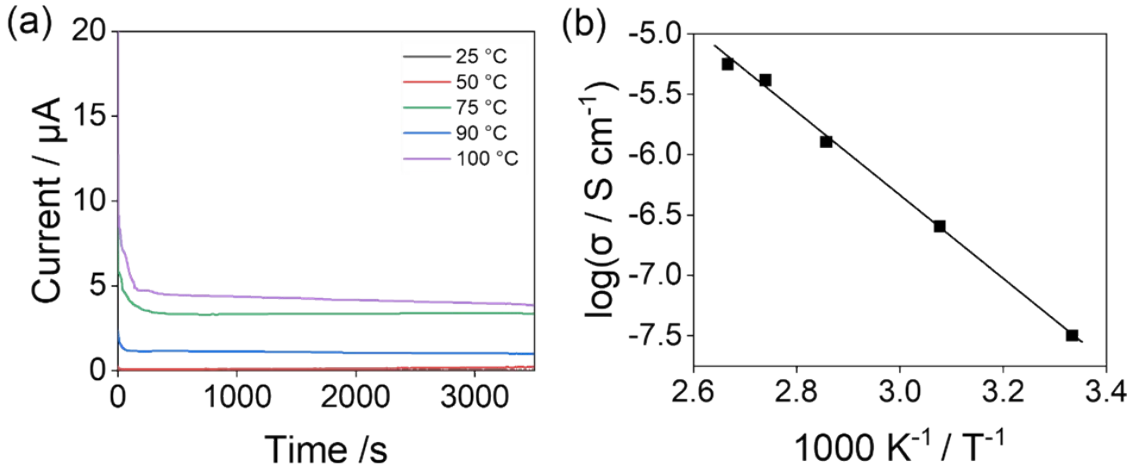

Figure S7. (a) Current-time curves of Cu/Li_3PS_4/Cu cells under direct current polarization at 100 mV. (b) Temperature dependences of electronic conductivity of Li_3PS_4.

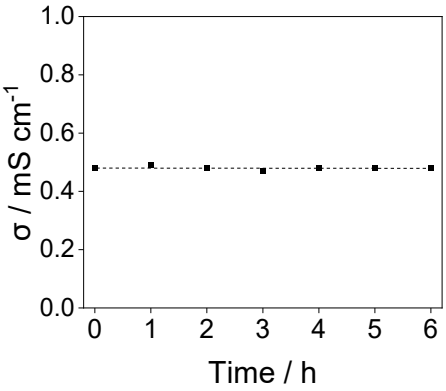

Figure S8. Time dependences of ionic conductivity of Li_3PS_4 solid electrolyte assembled in the operando cell (diameter of 1 mm) which was constant to 4.8×10^{-4} S cm^{-1}.

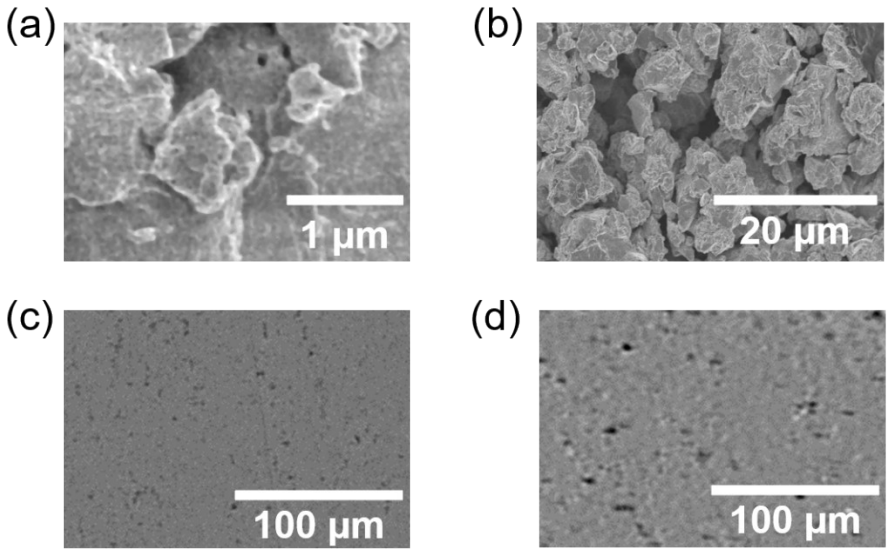

Figure S9. SEM images of (a) liquid-phase synthesized Li_3PS_4 and (b) solid-phase synthesized Li_3PS_4. Cross-sectional image slice taken from CT measurements of Li_3PS_4 pellet under 360 MPa using (c) liquid-phase synthesized Li_3PS_4 and (d) solid-phase synthesized Li_3PS_4, respectively.

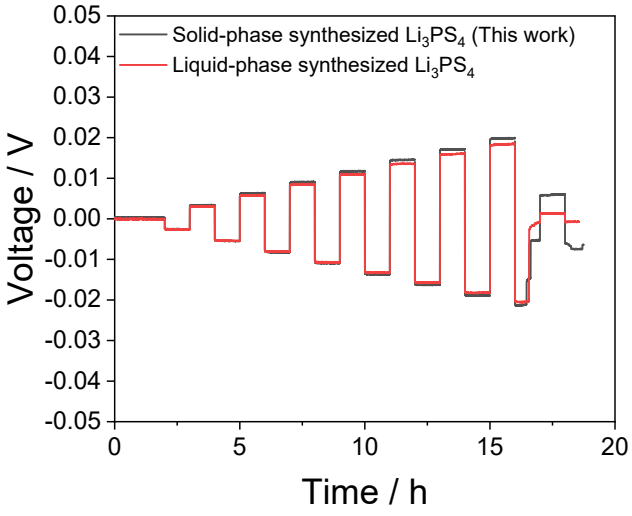

Figure S10. Critical current density test results for Li/solid electrolyte/Li cell using Li_3PS_4 synthesized via liquid-phase method and mechanical milling with current density increasing by 0.04 mA cm^{-2} after charging and discharging for 1 h at 25 °C. The inset arrow is an indicator of the ease of short-circuit caused by Li dendrite growth.

Table S1. Values used to compute V for Figure 1d.

Charging time (h)	Theoretical V of lithium (× 10^6 μm^3)	V of crack (× 10^6 μm^3)
0	0	0
0.5	1.4	0
1.0	2.8	0
1.5	4.1	0.11
3.2	8.8	3.2

Table S2. Time-based impedance parameters used for the fitting process to obtain the Nyquist plots in Figure S6.

Plating time (h)	R_{int} (Ω)	Q ($\times 10^{-7}$)	n	Capacitance ($\times 10^{-8}$ F)	R_{ct} (Ω)	Q	n	Capacitance ($\times 10^{-5}$ F)
0	5.1	6.5	0.82	4.5	15	0.00090	0.63	7.2
0.5	5.6	6.6	0.82	4.3	14	0.00088	0.59	4.2
1	5.9	6.4	0.82	4.3	13	0.00081	0.58	3.0
1.5	6.0	3.6	0.86	4.6	13	0.00079	0.52	1.0
2.5	6.8	1.7	0.92	3.5	12	0.00079	0.52	1.0

The theoretical V of lithium calculated above was used to clarify that the majority of crack is attributed to Li rather than voids, such that the equivalency can be described as follows:

$$Theoretical\ V\ (\mu m^3) = \frac{0.8\ mA/cm^2 \times (0.05\pi)^2 cm^2 \times n\ h}{3860\ mAh/g \times 0.59\ g/cm^3} \times 10^{12}\ \mu m^3/cm^3 \quad \text{(Equation S2)}$$

Each response in the Nyquist plots was fitted using a parallel R–CPE (constant phase element). The impedance of a CPE is calculated as follows[4].

$$C = R^{(1-n)/n} Q^{1/n} \quad \text{(Equation S3)}$$

where Q is a parameter independent of the frequency, n is an exponential factor, and C is the equivalent capacitance of the CPE.

Supplementary References

[1] A. Jain, S. P. Ong, G. Hautier, W. Chen, W. D. Richards, S. Dacek, S. Cholia, D. Gunter, D. Skinner, G. Ceder and K. A. Persson, *APL Mater.*, 2013, **1**, 011002.

[2] K. Yamamoto, S. Yang, M. Takahashi, K. Ohara, T. Uchiyama, T. Watanabe, A. Sakuda, A. Hayashi, M. Tatsumisago, H. Muto, A. Matsuda, and Y. Uchimoto, *ACS Appl. Energy Mater.*, 2021, **4**, 2275−2281.

[3] A. Kato, M. Yamamoto, A.i Sakuda, A. Hayashi, and M. Tatsumisago, *ACS Appl. Energy Mater.* 2018, **1**, 1002−1007.

[4] F. Yang, L. Li, P. Wu, E. Pradal-Velázquez, H. K. Pearce and D. C. Sinclair*, J. Mater. Chem. C,* 2018, **6**, 9258–9268.